OCL 2025, 32, 27
© P. Carré *et al.*, Published by EDP Sciences, 2025
https://doi.org/10.1051/ocl/2025023

OCL Oilseeds & fats Crops and Lipids

Available online at:
www.ocl-journal.org

RESEARCH ARTICLE OPEN ACCESS

Insights from an Instrumented Screw Press: Investigating pressure, torque, cage strain and flows dynamic☆

Patrick Carré[1,*], Florian Rousseau[1], Têko Gouyo[1] and Raphaëlle Savoire[2]

[1] Terres Inovia, 33600 Pessac, France
[2] Univ. Bordeaux, CNRS, Bordeaux INP, CBMN, UMR 5248, 33600 Pessac, France

Received 2 June 2025 – Accepted 17 July 2025

Abstract – This study presents a comprehensive, real-time investigation of the mechanical and flow dynamics within screw press during oil extraction from sunflower kernels and non-dehulled rapeseed. Using an instrumented press equipped with high-frequency sensors for pressure, torque, and cage strain, the research reveals pronounced cyclic fluctuations in internal pressures and deformations of the cage, closely tied to screw rotation. These findings challenge the adequacy of conventional steady-state models and highlight the need for dynamic approaches to capture the true behaviour of oilseed matrices during pressing. Comparative analysis demonstrates that sunflower kernels, due to their higher deformability and filtration resistance, exhibit flatter pressure profiles and reduced energy consumption, but also limit maximum pressure and oil yield compared to rapeseed. Residence time distribution measurements further uncover complex material flow patterns, including significant backflow at higher screw speeds, necessitating hybrid modelling approaches. The observed correlation between cage deformation and torque variation suggests that structural rigidity is a key factor for optimizing press performance and energy efficiency. Overall, this work advances the mechanistic understanding of screw press operation and provides new insights for improving oilseed processing efficiency and equipment design.

Keywords: Screw press / mechanical extraction / pressure

Résumé – Analyse d'une presse à vis instrumentée : étude de la pression, du couple, de la déformation de la cage et de la dynamique des flux. Cette étude présente une investigation en temps réel des dynamiques mécaniques et d'écoulement au sein d'une presse à vis lors de l'extraction d'huile à partir d'amandes de tournesol et de graines de colza. En utilisant une presse instrumentée équipée de capteurs haute fréquence mesurant la pression, le couple, la déformation de la cage et le couple. Cette recherche révèle des fluctuations cycliques marquées des pressions et déformations de la cage, étroitement liées à la rotation de la vis. Ces résultats remettent en cause l'adéquation des modèles conventionnels en régime permanent et soulignent la nécessité d'approches dynamiques pour décrire le comportement réel des matrices oléagineuses lors du pressage. L'analyse comparative démontre que les amandes de tournesol, en raison de leur déformabilité accrue et de leur résistance à la filtration plus élevée, présentent des profils de pression plus plats et une consommation énergétique réduite, mais limitent également la pression maximale et le rendement en huile comparativement au colza. Les mesures de distribution des temps de séjour mettent en évidence des écoulements complexes, incluant un reflux significatif à la vitesse de vis la plus haute, nécessitant des approches de modélisation hybrides. La corrélation observée entre la déformation de la cage et les variations de couple suggère que la rigidité structurelle est un facteur susceptible d'optimiser les performances et l'efficacité énergétique des presses. Globalement, ce travail approfondit la compréhension mécanistique du fonctionnement des presses à vis et offre de nouvelles perspectives pour améliorer l'efficacité du traitement des oléagineux et la conception des équipements.

Mots clés : presse à vis / extraction mécanique / pression

☆ Contribution to the Topical Issue: "Technological challenges in oilseed crushing and refining / Défis technologiques de la trituration et du raffinage des oléagineux".

*Corresponding author: p.carre@terresinovia.fr

This is an Open Access article distributed under the terms of the Creative Commons Attribution License (https://creativecommons.org/licenses/by/4.0), which permits unrestricted use, distribution, and reproduction in any medium, provided the original work is properly cited.

Highlights

- Real-time, high-frequency measurements in an experimental screw press reveal strong cyclic fluctuations in internal pressure, torque, and cage strain during oil extraction from sunflower kernels and rapeseed.
- Sunflower kernels show flatter pressure profiles and lower energy use but also reduced maximum pressure and oil yield compared to rapeseed.
- Residence time distribution analysis reveals important backflow of kernels.
- Observation of a strong correlation between cage deformation and torque variations.

1 Introduction

Mechanical screw pressing remains a critical yet energy-intensive step in global oilseed processing, accounting for over 30% of operational costs in decentralized plants, *i.e.* oil mill without solvent extraction (Kumar Metal, 2025). In conventional oilseed crushing units, mechanical extraction is an indispensable step for oil-rich seeds such as rapeseed, sunflower, and cotton, enabling the recovery of 60–70% of the oil (Ward, 1976; Booth, 2004; Le Clef and Kemper, 2015). This process is critical for preparing the seed material for the subsequent solvent extraction phase, as it conditions the physical state of the cakes. The structural integrity and porosity of these cakes are paramount to ensure uniform solvent percolation through the extractor bed and facilitate effective drainage prior to desolventization. Furthermore, the cold-pressing process for sunflower kernels is potentially applicable to produce protein-rich cakes, which could be used for demanding applications such as fish or piglet nutrition, or even for human consumption (Girotto, 2026).

With sunflower and rapeseed collectively representing 21.7% of global vegetable oil production (Pilorgé, 2020), optimizing these systems is relevant for meeting rising demand-projected to grow at 3.8% annually in the $17.1 billion oil extraction machine market (Future Market Insights, 2023). However, relatively few studies have investigated the parameters influencing the operation of mechanical extraction; most academic research has focused on laboratory-scale presses, which share few characteristics with industrial presses (Carré, 2022). Thus, contradictory results can be found, such as, for example, Bahadar *et al.* (2013) using a computerized model (ANSYS FLUENT) predicted higher pressure generation for higher rotation speed in contradiction with the results of Bogaert *et al.* (2018) who demonstrated with an instrumented press that increasing the rotation speed decreases the pressure measured at the cage level.

In the context of a study on the mechanical extraction of fully dehulled sunflower kernels, we were surprised to observe significant fluctuations in the current drawn by the press motor. This observation was made possible by the high-frequency acquisition of motor data (Rousseau *et al.*, 2025). The present study presents an investigation into dynamic interactions between torque fluctuations, cage deformations, and residence time distribution (RTD). While foundational work established basic pressure profiles in conventional presses (Vadke and Sosulski, 1988) and modeled RTD using axial dispersion approaches (Bogaert *et al.*, 2020), critical gaps persist in understanding real-time mechanical interactions during oil expression. As there is very little information available on material flow dynamics within oilseed presses, particularly regarding sunflower kernels, the observations presented here will advance the understanding of these press systems' operational mechanics.

Advances in instrumentation now enable the acquisition of high-frequency data, providing access to detailed information on observable relationships at the level of motor current fluctuations like it is currently performed with extruders (Barzegari and Almasi, 2020). To date, fluctuations in the resistant torque over a full rotation cycle of a press operating under steady-state conditions have never been examined. Similarly, variations in the pressure exerted on the frame and the stresses acting on the frame's retaining hoops (which are semicircular structures that secure the bars in place and are prone to deformation under stress) remain unstudied. Similarly, to the best of our knowledge, the residence time distribution in a screw press processing sunflower kernels has not yet been the subject of any published studies.

Such observations are relevant for refining models designed to predict the behavior of oilseed matrices within screw presses. For instance, Bogaert *et al.* (2018) draw a comparison between the screw press and a succession of piston presses functioning under constant strain rate, not accounting for the pressure variations during the screw rotation. Vadke *et al.* (1988) model assumes continuous compression without interruptions from the feed section to the ram section, unlike industrial screw presses with segmented worm assemblies and it doesn't consider the possibility of abrupt and cycling variations of compression parameters. Anferov and Skul'skiy (2014) presents a mathematical model of fluid filtration through a plastically deformable porous medium during rapeseed oil expression, using a two-component Eulerian approach to derive an approximate analytical solution showing exponential pressure increases along the extrusion channel in which the parameters evolve according to their progression in the channel without variations induced by the screw rotation.

2 Material and methods

2.1 Seeds and instrumented press

Sunflower kernels (SK) of the confectionery type were purchased in France from the commercial supplier Flanquart (Marles-les-Mines, Pas de Calais). The rapeseed used was a winter-type commercial batch obtained from a local cooperative.

The instrumented press utilized in this study was previously detailed in a forthcoming article (Rousseau *et al.*, 2025). In summary, the apparatus consists of an Olexa MBU20 screw press equipped with a segmented screw, as described in Table 1 and illustrated in Figure 1.

Table 1. Geometric information about the screw.

	A	*B*	*C*	*D*	*E*	*F*	*G*	*H*	*I*	*J*	*K*	*L*
Inlet diameter (mm)	68	68	73	73	81.5	81.5	84	84	86	86	89	89
Outlet diameter (mm)	68	73	73	81.5	81.5	89	84	91	86	95	89	93.5
Length (mm)	152	38	65	30	75	25	75	30	70	25	85	110
Rotation of the thread (°)	716		284		396		446		401		536	
Pitch of the screw	70		50		45		40		40		40	

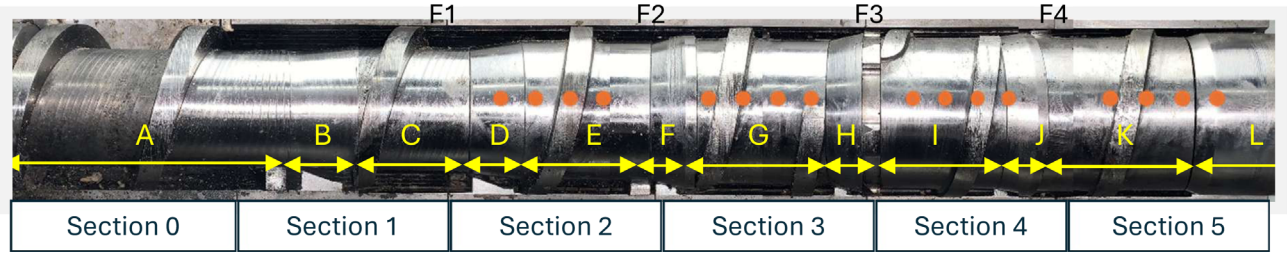

Figure 1. Picture of the worm assembly with the knives. The orange dots represent the position of the pressure sensors. The markers F1, F2, F3, and F4 indicate the position of clamping rings equipped with strain sensors – sections are the bar sections where oil flow rates were measured.

The instrumentation comprises four pressure sensors, each mounted on the final sections of the cage bars; these sensors can be positioned at various points spaced 20 mm apart. Between the gearbox and the screw is the thrust bearing that allows the transfer of axial thrust generated by the rotation of the screw to the cage and prevents the shaft from moving backwards. Between the thrust housing and the cage, a 200 kN annular force sensor (PM Instrumentation Model LWPF2) is placed to measure the thrust force. Four of the clamping rings (referred F1 to F4) are equipped with strain gauge (HBK 1-XY31-3/350), providing additional information on the outward pressure exerted by measure of the strain of the clamping rings with an accuracy of 1 µm in two orthogonal directions. The system also records data from the frequency converter, specifically the resistant torque and current intensity, at a frequency of 500 measurements per second.

2.2 Experimental procedure

All experiments were conducted using seeds or kernels held at ambient temperature. To obtain measurements at the four different pressure sensor positions, it was necessary to reposition the instrumented bar, which required stopping the press between each configuration. For each sensor position, a measurement cycle was performed following a specific sequence: the press first processed rapeseed at 3.5 rpm for 60 min, then at 7 rpm for 30 min. This was followed by the processing of sunflower kernels at 3.5 rpm for 30 min. The press then returned to rapeseed at 7 rpm for 30 min, and finally, sunflower kernels were processed again at 7 rpm. This protocol was designed to allow direct comparisons between materials and operating speeds while maintaining consistent experimental conditions.

2.3 Residence time distribution observations

Residence time distribution in the press was determined using the impulse tracer method. The tracer dye used was brilliant blue (CAS 6104-58-1, Sigma Aldrich, USA) prepared as an aqueous solution with concentration $C = 4.08$ g/L. Tracer impregnation was performed on a sample of 150 grams of kernels for 5 mL of brilliant blue solution. Three batches of 150 grams were prepared for each rotation speed. The seeds were mixed for 1 hour with a durabilimeter (a rotating square box) and left to rest for 48 h. The addition of 5 mL of solution increased the water content in the kernels from 4.6 % to 7.4 %. Although this moisture modification was likely to modify the behavior of the kernels in the press, it was assumed that this would not affect the general displacement of the unmarked kernels.

The injection of the marked kernels was made once the press was reaching steady state (pressure and temperature remaining between 57 °C and 58 °C for 10 min). The injection was performed when the screw became almost empty in the feeding zone. The press was then refed as usual. Cake samples were collected at the press outlet every 5 seconds from 0 to 480 seconds after the marker introduction at 3.5 rpm, and from 0 to 280 seconds after the kernels introduction at 7 rpm. Each sample was collected by taking the entire cake output from the press over a 5-second period. The collected mass ranged between 5 and 15 grams. The measure of residence time distribution was repeated 3 times for each rotation speed.

2.3.1 Tracer concentration measures

Three grams of oilcake were inserted into a pillbox and soaked in 15 mL of a 70:30 v/v ethanol/water mixture. The mixtures were shaken vigorously by hand every 5 minutes for 20 minutes. After settling, the liquid was collected and centrifuged for 5 minutes. Two milliliters of clarified solution were collected and placed into a 30 mm white cup. The tracer concentration in the sample was measured using a colorimeter (PCE Instruments, Germany) that expresses colour in the Lab colour space. As our tracer was a blue dye, only the 'b' value was considered. Due to some heterogeneity in the maximum

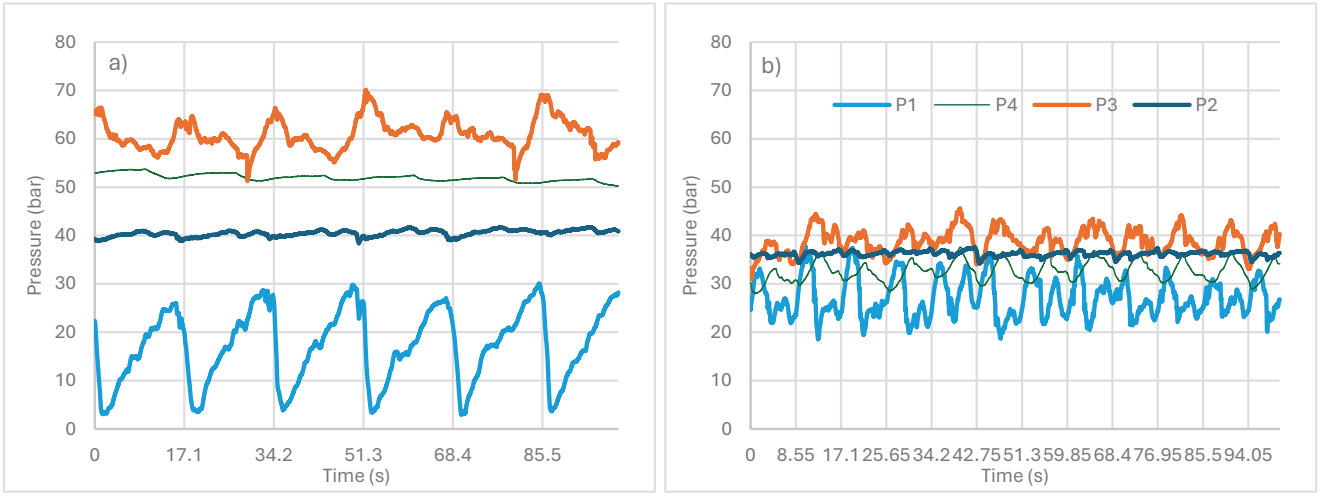

Fig. 2. Evolution of the pressure under steady state with sunflower kernels at (a) 3.5 rpm ; (b) 7 rpm with the sensor in position A2.

values obtained, the results were normalized by dividing all values in each series by their maximum value.

The simulation used an Excel spreadsheet with each row representing one second. For plug flow reactors, two columns tracked incoming and outgoing tracer flows; outgoing flows were calculated using the 'INDIRECT' function, referencing the incoming flow column at a row offset by the residence time. For perfect mixers, four columns were used: incoming flows (from upstream reactors), tracer stock (previous stock + incoming − outgoing), tracer concentration (stock divided by material stock, the latter being residence time × sunflower kernel flow), and outgoing tracer flow (concentration × material flow). A scale parameter adjusted model outputs to match observed coloration intensity. The Excel GRG nonlinear solver minimized the squared deviation between observed and modelled tracer exiting the last reactor by optimizing reactor characteristics.

3 Results

3.1 Measures of the pressure

Pressure was measured simultaneously at 4 points on the press. Figure 2 shows a representative 100-second sample for each rotation speed, and each graduation represent a rotation of the screw (17.1 seconds for 10 Hz and 8.55 seconds for 20 Hz), with the pressure transducers in position A2, P1 to P4 correspond to measures made in the area of worms 'E', 'G', 'I' and 'K' (Fig. 1) respectively corresponding to last four sections of bars.

At 3.5 rpm, significant pressure variations in P1 were observable, ranging from a minimum of 2 bar to a maximum of around 30 bar. The pressure increased linearly for about 13 seconds, before dropping abruptly. Similar pressure variations were evident in the third cage section, where pressure rarely dropped below 55 bar, and reached peaks of about 70 bar (P3 orange curve on plot). However, these peaks were not as regular as for P1. With P3, pressure maxima were separated by periods of steady pressure. In sections 2 and 4, pressure variations were more limited. The periodicity of the variations corresponds to the rotational speed of the screw, which at 3.5 revolutions per minute results in 17.1 second cycles. These variations are related to the distance between the screw thread and the measurement point. We observe that the maximum pressures for P1 and P3 occur almost simultaneously, suggesting that in these two situations, the screw thread passes in front of the measurement points at the same moment, which is confirmed by the observation in Figure 1 (edge of the thread and third orange dot of 'E' and 'I' screw segments). A similar phenomenon is observed for P2, but not for P4.

At 7 rpm (b plot), P1 pressure cycled between pressure maxima (35 bar) and minima (20 bar) in a more irregular manner. Surprisingly, the pressure was cycling twice within one period. Pressure P3 was also cyclical, ranging between 35 bar and 45 bar. The 2 slopes around the peak were symmetrical, though irregular. Pressure P2 was stable at around 35 bar while P4 presented also cyclical variations between 30 and 35 bar.

In terms of absolute values, the two rotation speeds were distinguished by divergent evolutions. At 3.5 rpm, these values are spreading from, 2 bar to 30 bar for P1, 40 bar for P2, 46-68 bar for P3 and around 50 bar for P4. At 7 rpm, all the pressures varied within the range 23 to 45 bar.

3.1.1 Measures of the pressure

This part reproduces a part of the results already published in Rousseau *et al.* (2025) for reason of clarity. Figure 3 represents the concatenation of the pressure measures made on the cage for each position of the sensors. The boxes are delimited by the average maximum and minimum pressures measured at a single point. The lines extending from the boxes represent the standard deviation of these pressure measurements. The broken line passing through the centre of the boxes represents the evolution of the median pressure point. Table 2 recapitulates these values.

The semi-circular frames of the cage created interruptions in the measurement points. As a result, pressure readings could not be taken at consistent 20 mm intervals. Consequently, the broken lines representing the pressure data in the graph are also discontinuous at these points. To avoid overlapping of the data figures, the boxes for the 7 rpm series were slightly offset to the

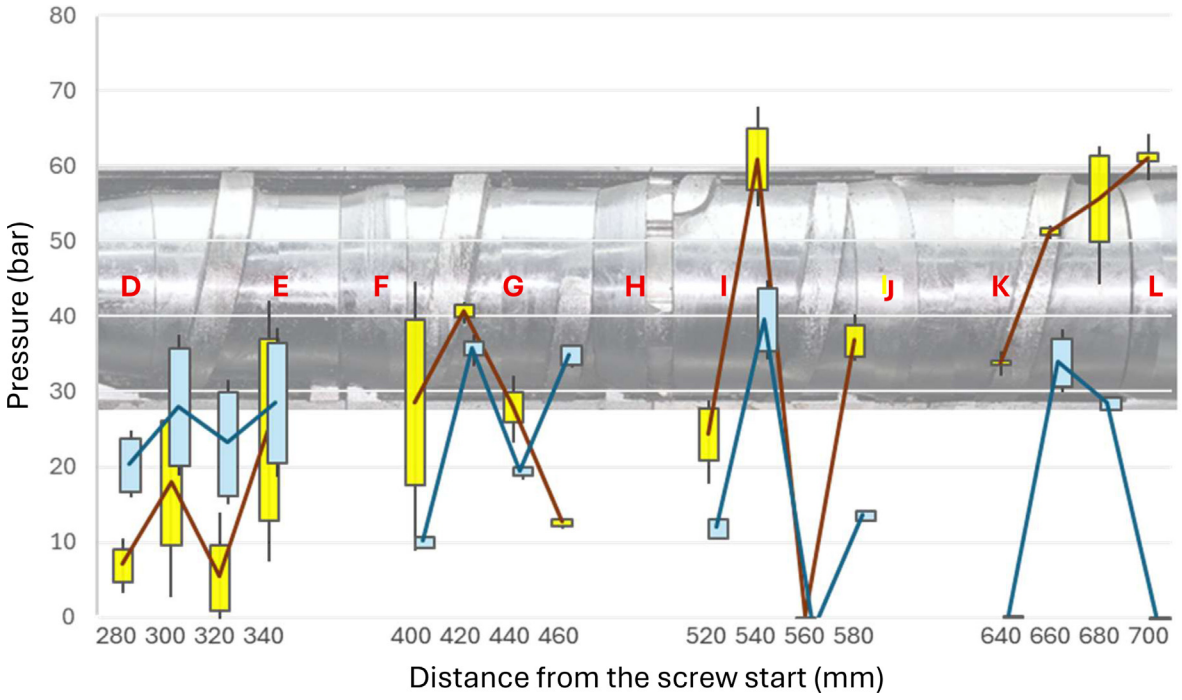

Fig. 3. Representation of the pressures measured at 16 locations on the cage at 7 rpm (blue lines and boxes) and 3.5 rpm (brown line, yellow boxes) in the processing of sunflower kernels. The boxes present average minimal and maximal pressure, during one rotation of the screw the whiskers the standard deviation of these data. Broken lines join the midpoint between these values. The boxes present average minimal and maximal pressure.

Table 2. Pressure sensor data: Mean values of midpoints and amplitudes ranges for positions A1 through A4 at rotational speeds of 3.5 and 7 rpm.

Pressures (bar)			P1	P2	P3	P4
Midpoint	3.5 rpm	A1	6.8	28.5	24.3	33.8
		A2	17.8	40.7	60.9	51.2
		A3	5.2	27.9	-0.3	55.6
		A4	24.9	12.6	36.7	61.2
	7 rpm	A1	20.5	10.2	12.0	0.3
		A2	28.2	36.0	39.8	34.1
		A3	23.3	19.6	-1.7	28.6
		A4	28.7	35.0	13.7	0.1
Amplitudes	3.5 rpm	A1	4.5	21.9	6.9	0.5
		A2	16.5	1.8	8.1	0.9
		A3	8.7	4.1	0.1	11.5
		A4	24.2	0.9	4.1	1.0
	7 rpm	A1	7.2	1.5	2.5	0.1
		A2	15.6	1.8	8.2	6.3
		A3	13.9	1.2	0.4	1.5
		A4	16.1	2.5	1.1	0.1

right. The midpoint is the medium point between the maximum and the minimum value of pressure, and the amplitude is the the difference between the maximum and minimum pressure values.

The area 280 to 340 mm (P1) is characterized by the largest amplitudes of pressure at both rotational speeds with an average amplitude of about 13 bar. From 400 to 460 mm (P2) these amplitudes were strongly reduced at 7 rpm (1.7 bar) while it remained larger at 3.5 rpm, a mean mainly due to the measure at 400 mm. In the third area (520-580 mm, P3), average amplitude was 4.8 bar at 3.5 rpm and 3.1 bar à 7 rpm. A remarkable pressure drop was observed in position A3. In the last area (640-700 mm, P4) the amplitudes are heterogenous with a maximum in position A3 at 3.5 rpm and A2 at 7 rpm.

Figure 4 presents the same data in the case of rapeseed pressed in the same conditions. In the first screw segment,

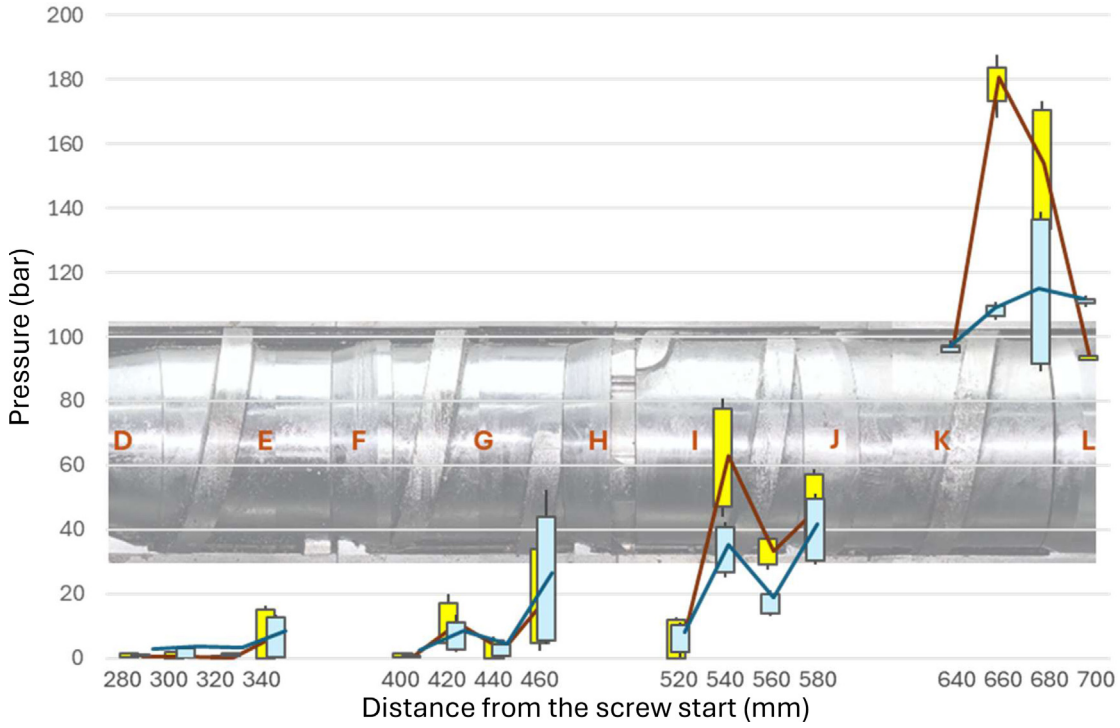

Fig. 4. Representation of the pressures measured at 16 locations on the cage at 7 rpm (blue lines and boxes) and 3.5 rpm (brown line, yellow boxes) in the processing of rapeseed. The boxes present average minimal during one rotation of the screw the whiskers the standard deviation of these data. Broken lines join the midpoint between these values.

rapeseed generated very low pressure (P1) in the position A1 to A3 and pressure started rising up to 15 bar only in position A4 for both rotational speeds. In the following screw segment, the pressure (P2) remains low in positions A1 to A3 and cycles between 5 and 33 bar at 3.5 rpm and from 5 to 43 bar at 7 rpm in position A4. Crossing the serrated ring 'H' with its serrated crown cause a pressure drop in P3-A1 of the screw 'I' (520 mm). The pressure rises significantly at the position P3-A2 with a more dramatic jump at 3.5 rpm (47-77 bar) than at 7 rpm (26-40 bar). In position P3-A3, a drop was observed but which was not as important as with SK. In position P3-A4, the pressure rose again without going to the same levels as in position A2. In the screw segment 'K', the pressure (P4) reached values between 100 and 180 bar much higher than with SK. At 3.5 rpm, the maximum pressure (173–183 bar) was observed in position A2 and in position A3 for 7 rpm (91–135 bar).

These strain measurements on the clamping rings also allow us to dismiss the hypothesis that the low pressures measured at position P3-3 could result from a deviation in experimental conditions, as the strains in F3 and F4 of the third series are not significantly different from those measured during other experiments.

3.2 Strain of the cage

Figure 5 presents the evolutions of the strains measured on the clamping rings F1 to F4 in two perpendicular directions referred as A and B during the experiment A2. Vertical axis on the left represents the strain in μm in the A orientation, the opposite the strain in the B orientation. Absolute values express opposite deformations with a compression in one direction and an extension in the other. As for the pressure, the variations are cyclic and are related to the rotation of the worm. These variations are complementary as it is clearly visible for the F4 measures. Maximal and minimal values of the strain in orthogonal directions are occurring at the same time which is logical since the deformation of the clamping rings is happening in both orientations when the force exerted by the cake on the cage tends to ovalize the circle of the clamping rings.

Table 3 recapitulates the midpoints between mean minimal and maximal strains and the amplitudes of variations of the strains during the cycles in the two orientations and for each rotational speed. At 3.5 rpm, the general evolution of the pressure and strain are marked by a common progression from upstream to downstream. Considering the mean of the pressure for each cage section and the magnitude of the resultant vector of the two strain measures which can be calculated using the Pythagorean theorem, for each additional bar of pressure, an increase of about 4 μm of the resulting strain vector (RSV) is observed. At 7 rpm, the average pressure measured in P1 and P2 is superior to the pressure measured in P3 and P4 while the RSV are growing from 51.5 μm in F1 up to 134.8 μm in F4. The amplitude of the RSV variations was correlated with the RSV (R^2= 0.92) meaning that when the deformation increases by 4.25 μm, an increase of 1 μm in the amplitude of this deformation is observed. Beside this general trend, sometimes, the amplitude may vary more as for example in F2 at 3.5 rpm with 36.5 μm of amplitude for 91.6 μm in RSV and less like in F3 at 3.5 rpm with an amplitude of 26.3 μm for 146.8 μm in RSV. The same trend is observed at 7 rpm for the clamping rings F2 and F3.

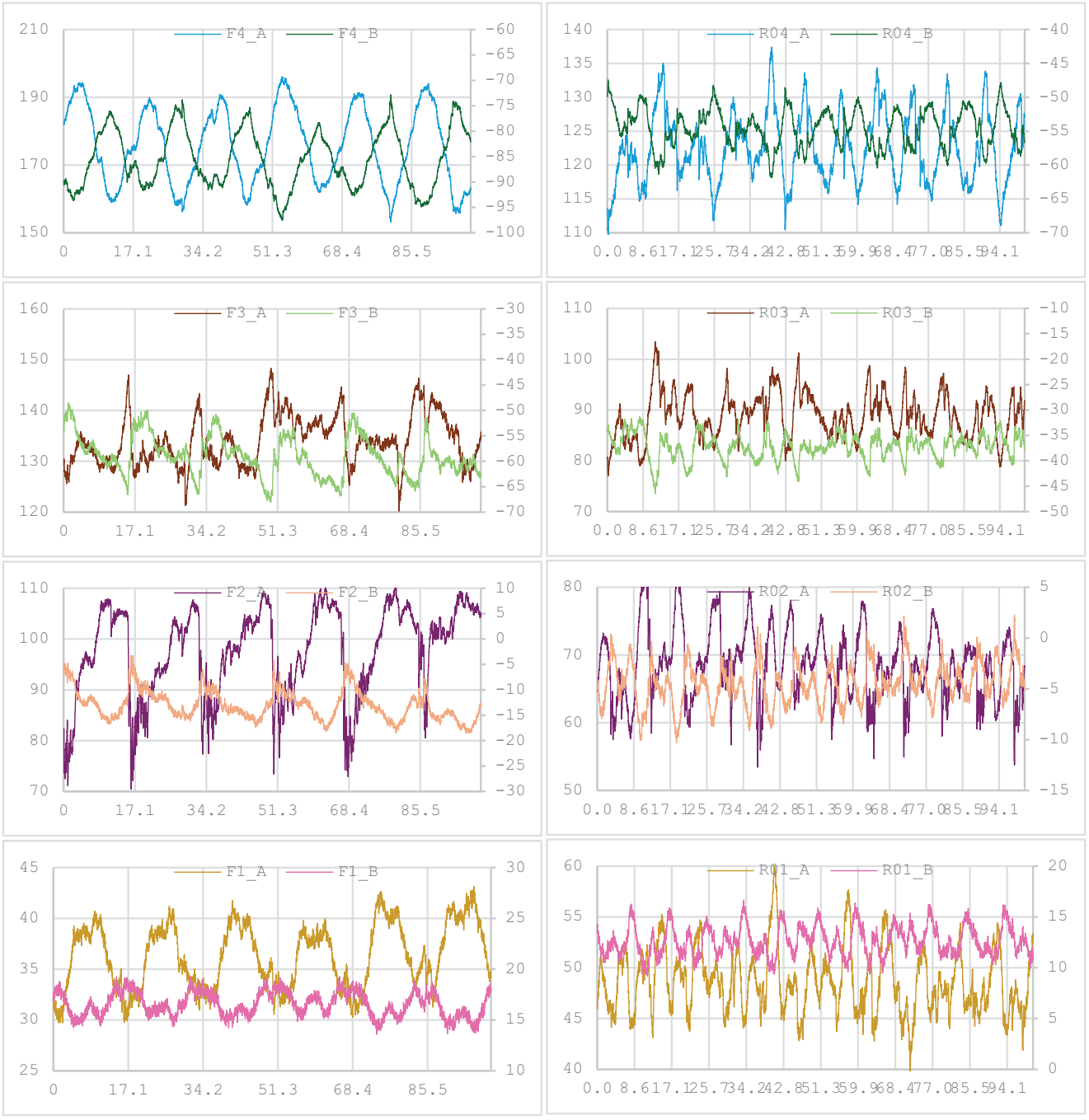

Fig. 5. Strain variations of the clamping rings at two rotational speeds (3.5 rpm on the left, 7 rpm to the right). Vertical axis express the amplitude of the clamping ring strain (μm) left axis represents the strain of the A orientation, right axis the B orientation. Experiment A2.

Figure 6 shows the strains measured at two rotational speeds for the four experiments during which the locations of the pressure sensors were modified from position A1 to A4. The boxes are delimited by the average minimal and maximal strains and the whiskers the standard deviation of these means. For each clamping ring, the four results are presented side-by-side in the order A1 to A4.

The global evolution of the strain presents similitudes with the evolution of the pressures. Strain and pressure are higher for sunflower in the left part of the press (F1, F2) but lower in the last section where rapeseed strongly differentiates itself from sunflower (F4). The change in rotational speed leads to lower strains for rapeseed as for SK.

Table 3. : Evolution of the strain on the clamping rings and their amplitudes at 3.5 and 7 rpm during experiment A2 (μm).

Observation	Speed	Orientation	F1	F2	F3	F4
Midpoints	3.5 rpm	A	36.2	90.9	134.8	175.7
		B	16.5	-11.3	-58.1	-84.9
		$(A^2+B^2)^{0.5}$	39.8	91.6	146.8	195.1
	7 rpm	A	49.9	67.7	89.8	123.3
		B	12.7	-4.4	-37.6	-54.4
		$(A^2+B^2)^{0.5}$	51.5	67.8	97.4	134.8
Amplitudes	3.5 rpm	A	11.1	34.3	20.9	35.7
		B	4.9	12.6	16	19.1
		$(A^2+B^2)^{0.5}$	12.1	36.5	26.3	40.5
	7 rpm	A	12.2	19.8	16.2	18.9
		B	6.2	8.2	9.5	9.9
		$(A^2+B^2)^{0.5}$	13.7	21.4	18.8	21.3

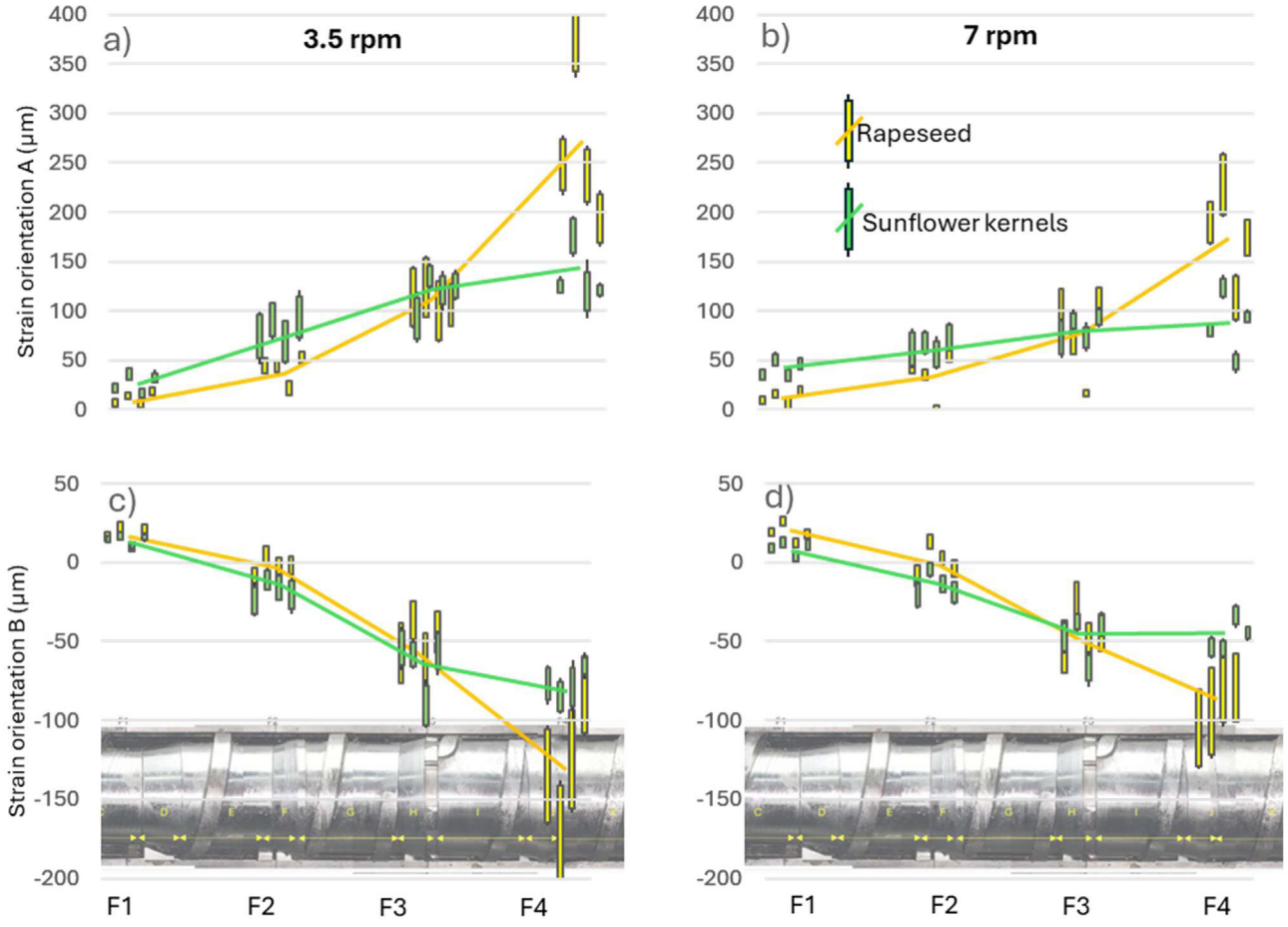

Fig. 6. Comparison of clamping rings strains for rapeseed and sunflower at two rotational speeds. a) 3.5 rpm, strain in the orientation A. b) 7 rpm, strain in the orientation A. c) 3.5 rpm, strain in the orientation B. d) 7 rpm, strain in the orientation B. The boxes present average minimal and maximal strain, the whiskers the standard deviation of these data. Broken lines join the midpoint between these values.

These strain measurements on the clamping rings also allow us to dismiss the hypothesis that the low pressures measured at position P3-3 could result from a deviation in experimental conditions, as the strains in F3 and F4 of the third series are not significantly different from those measured during other experiments.

3.3 Torque and intensity called to the motor

Figure 7 compares the evolutions of the torque and the intensity measured by the frequency invertor during experiment A2. The power results from a calculation taking into account the frequency and the value of the torque Eq. (1).

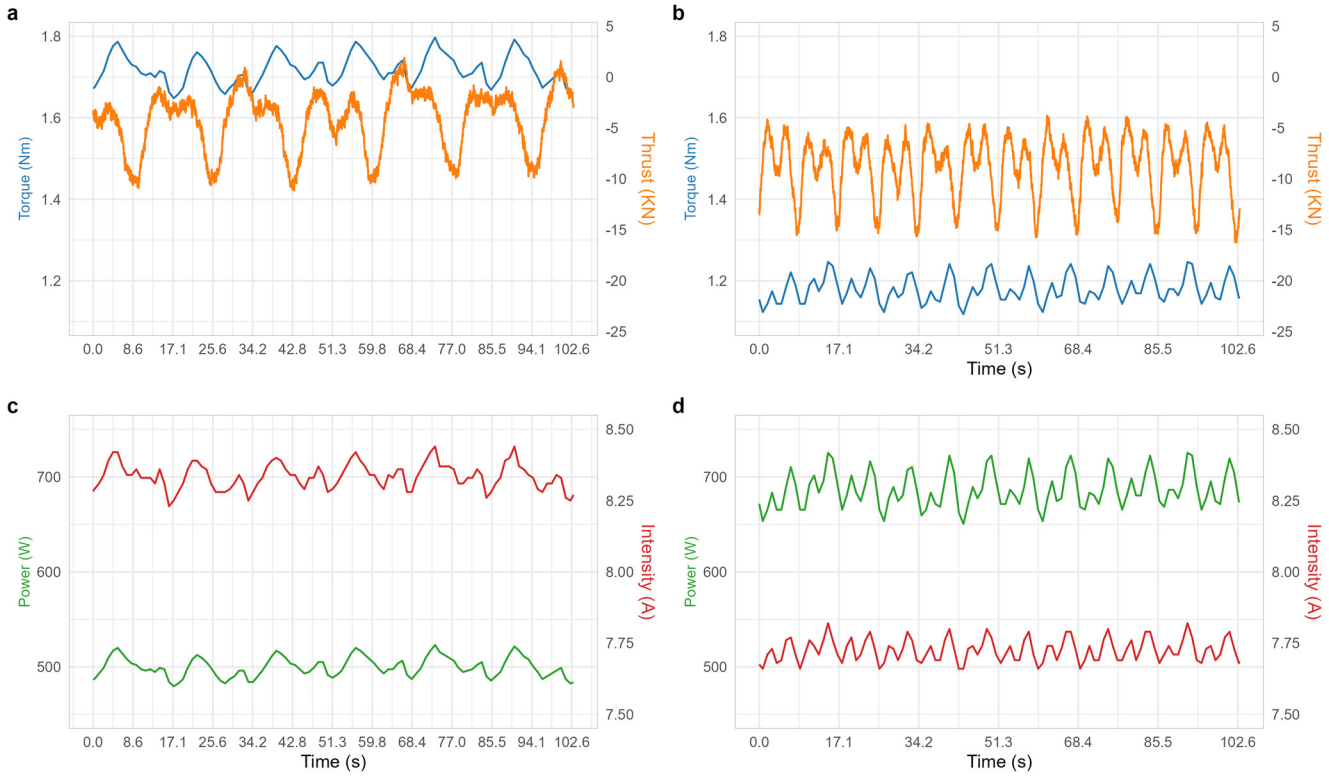

Fig. 7. Evolutions of the torque and the force exerted on the thrust (top), the current, the power (bottom) bearing at 3.5 rpm (a), and 7 rpm (b) for 100 s during experiment A2 (sunflower kernels).

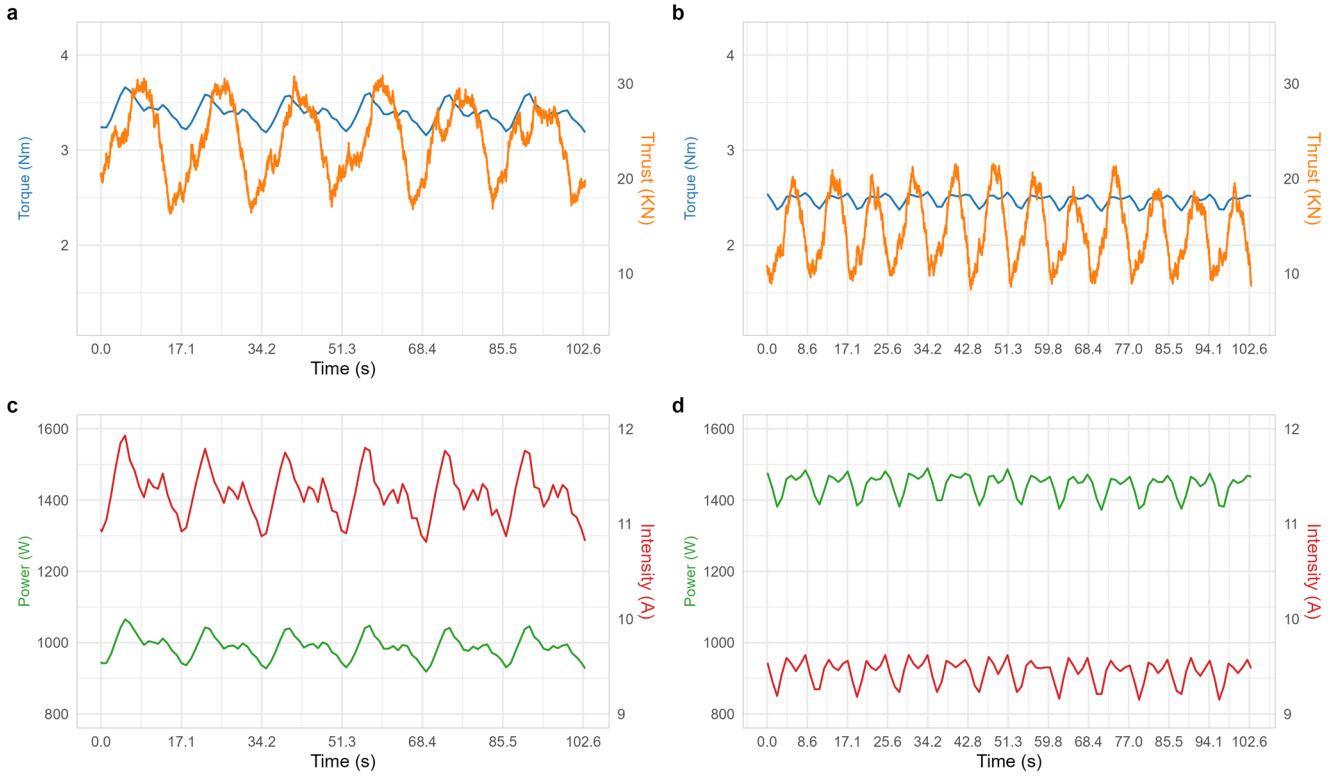

Fig. 8. Evolutions of the torque and the force exerted on the thrust (top), the current, the power (bottom) at 3.5 rpm (a), and 7 rpm (b) for 100 s during experiment A2 (Rapeseed).

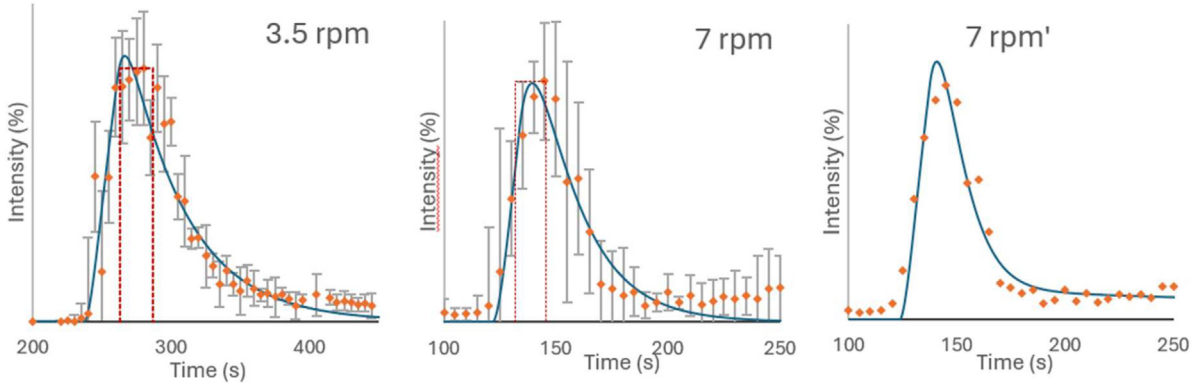

Fig. 9. distribution of the residence time and its modelling at 3.5 et 7 rpm (simple model) on right alternative modelling for 7 rpm.

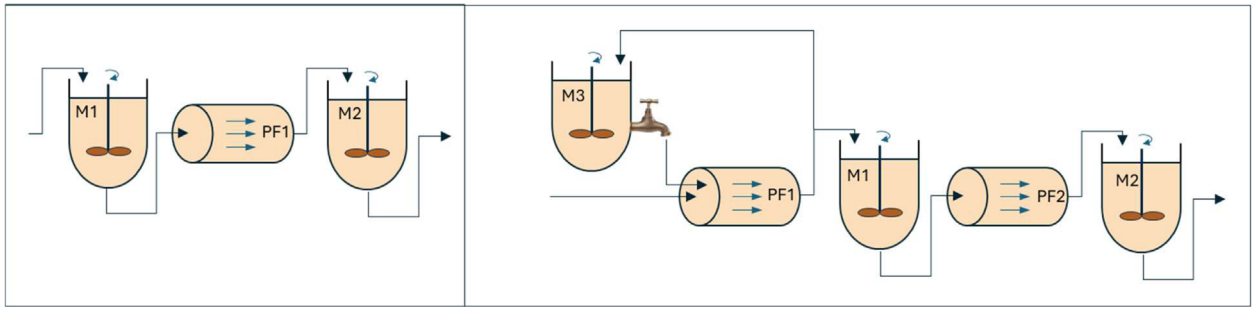

Fig. 10. Diagram of the residence time distribution modelling: left, simple model, right model 2 with retention of backflow used for 7 rpm' in Figure 9.

$$P = T \cdot \frac{F}{50} \cdot 1455. \quad (1)$$

With P = power (W), T = Torque (Nm), 'F' = frequency (Hz), 1455 = speed of the motor at 50 Hz.

Surprisingly, the thrust measured with the force sensor mounted on the thrust bearing was giving negative values during the crushing of SK. This indication is curious given that when the press was running without material, the values were correctly close to zero and positive when rapeseed was pressed (Section 4.2). Like with pressure and strain measured on the clamping rings, the force observed on the thrust bearing was varying with each revolution of the screw. The curves are very similar for both rotational speed with two peaks separated by a relatively important drop occurring only once per cycle.

Torque presents also some variation during the revolution of the screw, but their amplitudes are relatively limited. Intensity variations are very similar to the variation of the torque. While the press is running in absence of material, the torque has a value of 0.56 Nm and the intensity a value of 7.53 A. Between 3.5 rpm and 7 rpm, the power shift of about 160 W while the intensity drops due to the higher frequency.

Figure 8 presents the same data as Figure 7 for rapeseed processed in the same conditions. Compared to SK, rapeseed generates much more resistance to the screw rotation. It is visible at both rotational speeds with higher values for the force measured at the thrust bearing (negative values for SK versus 17–30 kN for rapeseed at 3.5 rpm and 10–20 kN at 7 rpm). Torques also are strongly differing with values which are about twice those of SK. In terms of motor current (intensity called to the motor), the differences are not so large with measures around 8.3–8.4 A for SK at 3.5 rpm versus 8.3–8.5 A with rapeseed. At 7 rpm the data diverge with 7.7–7.8 A vs. 9.2–9.5 A for SK and rapeseed respectively. The same evolution is visible for the power: small difference at 3.5 rpm (~500 W) larger at 7 rpm: 650-700 W *vs.* 1400-1500 W.

3.4 Residence time distribution (RTD)

The assessment of residence time distribution provides insight into the flow patterns of material from one screw segment to another. Figure 9 illustrates the results and their variability derived from three replicate measurements at two different rotational speeds. The dotted rectangle indicates the theoretical variation in tracer intensity that would occur if the flow had assumed the form of a single plug flow reactor. In this case, the initial appearance of the tracer is calculated by estimating the number of screw rotations required for a particle positioned at the exit of the feeding zone to reach the press outlet. To achieve this, it was assumed that in segments without screw flights, specifically the cone rings, the displacement velocity was imparted by the upstream screw and remained constant throughout these segments. Considering that the feeding zone occupies the first 100 millimetres of the screw, this calculation yields an estimated transit time of 261.2 and 130.6 seconds for rotational speeds of 3.5 and 7 rpm, respectively.

Table 4. Estimators of the residence time distribution of the model and R^2

	3.5 rpm	7 rpm	7 rpm'			
RT in Mix1	43 s	20 s	RT in PF1	9 s	RT in M2	8 s
RT in PF2	232 s	113 s	RT in PF2	98 s	K_1 Rate of flow to M3	63%
RT in Mix2	6 s	7 s	RT in M1	9 s	K_2 Rate exit from M3	0.29%
R^2	95.2%	94.2%				96.4%

The modelling of the residence time distribution was made using the diagram presented in Figure 10, with a succession of two perfectly mixed reactors separated by one plug-flow reactor. In a plug-flow reactor, the concentration of tracer is conserved at the end of the transit period. In a perfectly mixed reactor, the tracer is immediately dispersed in the mass of the reactor and the concentration at the outlet is those of the whole reactor.

The model selection was based on the principle of minimizing complexity while maximizing the quality of the prediction estimated by the R^2 between predicted values and observed values. This optimal result was achieved using only three successive reactors. However, this model does not adequately account for the observation at 7 rpm, where a recurrent presence of tracer in limited quantities over time is inconsistent with the model predictions. Figure 9 also illustrates a higher variability in the observations made at 7 rpm, as represented by the error bars. Table 4 presents the estimators for the model that minimizes the sum of squared deviations. With the exception of the residence time in the second perfect mixer, both models exhibit similar characteristics, with times approximately halved for the higher speed. However, it is visually apparent that the 7 rpm model does not fit well towards the end of the curve. Indeed, a persistence of the tracer is observed, which could be attributed to retention in the feeding zone and subsequent slow release, explaining this prolonged coloration. To address this discrepancy, a second model, illustrated in Figure 10 (7 rpm'), was tested. This model incorporates an additional plug flow stage (PF1) preceding the M1 perfect mixed reactor, with the flow divided into two streams: the primary stream entering mixer M1, and the secondary stream directed to mixer M3. K_1 represents the partition coefficient towards M3. Mixer M3 can accumulate the tracer without limitation and releases it towards the entrance of PF1 according to the equation (2)

$$\dot{M}_i^t = M_i^t \cdot K_2, \tag{2}$$

where M_i^t is the mass of tracer in M3 at the time i, $\dot{M}_i^t$ is the flow of tracer at the same time, K_2 is the rate of release for the tracer from M3. The second model slightly improve the determination coefficient R^2 (96.4 *vs.* 94.2%) and gives a more satisfactory prediction of the remanence of the tracer at the end of the experiment. This model finds additional support in the observed differential of blue coloration as measured by the colorimeter. The intensity difference is more pronounced at 3.5 rpm compared to 7 rpm (25.7 ± 4.9 *vs.* 11.8 ± 0.5 blue units for 3.5 and 7 rpm, respectively). This discrepancy can be partially attributed to the higher oil content in the cake produced at 7 rpm. However, this difference in oil content accounts for only approximately two-thirds of the observed decrease in coloration intensity. The remaining variation suggests that additional factors, beyond oil content, may influence the tracer dynamics and coloration at different rotational speeds.

4 Discussion

4.1 Pressure dynamics in mechanical extraction of sunflower kernels

Beyond the insights this experimentation has provided regarding the challenges of mechanical extraction applied to low-fiber matrices, several additional inferences can be drawn. These include observations on pressure evolution as a function of rotational speed and matrix composition, the relationships between pressure and clamping rings strain, and pressure variations during a single rotation cycle. These findings contribute to a more comprehensive understanding of the complex dynamics within screw presses during oil extraction processes.

4.1.1 Pressure profiles

To the best of our knowledge, this study is the first to provide such a detailed view of the pressures measured on the press cage, complemented hoop by clamping ring. Our predecessors (Vadke and Sosulski, 1988; Bargale *et al.*, 1999; Bogaert *et al.*, 2018) demonstrated that pressure is generally higher near the cake outlet zone and that a reduction in speed leads to increased pressure. However, no previous research has revealed the significant pressure fluctuations observed in this study with sunflower kernels, between P1 to P4. Similarly, the representation of pressure variations at a single measurement point has never been presented to the public in the manner we propose here.

In this study, we observed that an increase in rotational speed is not always accompanied by a decrease in pressure, as evidenced by consistently higher pressures at the 'E' screw segment at 7 rpm (P1). This observation can be readily linked to the phenomenon of increased filtration resistance in low-fibre matrices, which results in higher pressure under conditions of faster compression (Fig. 2).

4.1.2 Pressure fluctuations

Another aspect to consider is the comparison of pressures between the rear and front portions of the screw segments. One would expect to find the highest pressures towards the screw outlet due to the proximity between the thread and the

restriction imposed by the downstream conical ring. Paradoxically, this is not what is observed in certain screw sections. For instance, with the 'G' segment, the highest pressure with SK is observed at position 2, which is 25 mm from the beginning of this segment. The same phenomenon is observed in section 'I', where position 2, located 50 mm from the start, shows the highest pressures. Another illustration of this is visible in Figure 4, where the same dynamic is present in segment 'I' (P3) for the lowest speed, with a decrease in pressure observed from position 2 to position 3. Recalling that screw 'E' is dominant at 3.5 rpm, with sunflower kernels it is noteworthy that the pressures at P2-1 exhibit significant similarities with those at P1-4. This observation suggests that the passage through cone 'F' did not result in relaxation at the entrance of screw 'G', despite its diameter being smaller than the largest diameter of cone 'F'. The fact that the pressure at P2-2 does not experience fluctuations and remains consistently around 40 bars seems more challenging to explain. The absence of pressure fluctuations during rotation cannot be explained by the sensor's position, which encounters material pushed by the front face for 30% of the time, material arriving at the rear of the thread for 36%, and the thread top surface for the remainder. The lack of fluctuations under these conditions is therefore difficult to comprehend and cannot be attributed to the formation of a plug at the sensor location, as significant pressure fluctuations are observed on sensor P2 when rapeseed is processed during the same experimentation.

Another intriguing observation is the presence of zero pressure values at certain locations, such as P3-3 at both rotational speeds, and P4-1 and P4-4 at 7 rpm. We can dismiss the hypothesis that these sensors malfunctioned during the experiments where these values were recorded, as these same sensors registered significant pressures when rapeseed was processed in the press between each SK rotational speed trial. Furthermore, we have strain measurements from the clamping rings, which indicate that the internal pressure in the cage was not significantly different compared to experiments conducted when the sensors were in other positions.

These observations lead us to propose a hypothesis based on Raβ's thesis, which utilized a unidirectional press apparatus capable of simultaneously measuring the force exerted on the piston and the pressure at the base of the compression chamber. Raβ asserts that the force exerted by the piston reflects the pressure applied to the solid material, while the pressure measured at the chamber's base reflects the liquid pressure. Extrapolating this concept to our screw press, we could posit that the sensors positioned on the cage measure the oil pressure, whereas the deformation of the clamping rings would more accurately represent the pressure exerted on the cake. This hypothesis could potentially explain the absence of pressure observed when the press is not producing oil while the strain on clamping rings prove the presence of some pressure on the cake.

4.1.3 The effect of the matrices on the pressures profiles.

A comparison between rapeseed and sunflower kernels (Figs. 3 and 4) reveals contrasting pressure evolutions for these two matrices. The SK profile is notably flatter than that of rapeseed, where pressure remains very moderate for screws 'E' and 'G', average for section 'I', and significantly higher for segment 'K'. This evolution aligns with the description provided by Vadke and Sosulski for canola, with several values exceeding 100 bars. These data are corroborated by the strain measurements on the clamping rings (Fig. 6), which demonstrate lower strain values for rapeseed in the first two sections, equivalent values in the third, and markedly higher values for rapeseed on the last hoop. This pattern holds true for both rotational speeds, with the effect of higher speed being fairly comparable for both matrices.

These observations partially align with the primary hypothesis of this study, which attributes the difficulties in pressing sunflower kernels to their lower filtration resistance compared to undehulled rapeseed. In the initial compression phases, the pressure in the rapeseed cake is relatively low as oil circulates easily through the cake, generating minimal pressure. However, this hypothesis alone is insufficient to explain why rapeseed ultimately generates higher pressures. When the residual oil quantity becomes low, the determining factor for pressure is likely related to the cake's plasticity, or its capacity for deformation as defined by Carré (2022). The SK cake is more readily deformable and can flow towards the outlet, which limits the press's ability to generate pressure and, consequently, restricts its oil extraction capacity. This represents another aspect of the role of hulls in press cakes, acting as reinforcing elements that contribute to the mechanical strength of the material.

4.2 Torque, power and force on the thrust bearing

4.2.1 Torque comparisons

The resistive torque reflects the amount of energy required to press the oleaginous matrices. The difference between rapeseed and sunflower kernels is substantial, with significantly higher values observed for rapeseed compared to sunflower kernels at both rotational speeds. The effort required to press rapeseed is thus markedly superior, particularly at 3.5 rpm. This result demonstrates that when dehulled matrices are not penalized by their filtration resistance issues, their lower resistance to compression becomes advantageous in terms of energy consumption. Developing a screw design adapted to these matrices could potentially lead to significant savings in pressing energy consumption. Several authors support this assertion: Uitterhaegen and Evon (2017) reported that dehulling coriander fruits prior to mechanical pressing resulted in significant saving from 463 kWh/t to 221 kWh/t, Karaj and Müller (2011) with Jatropha curcas found that dehulling the seeds prior to pressing resulted in a 20% reduction in specific energy consumption.

4.2.2 Torque variations

The change in rotational speed has a pronounced effect on the motor's resisting torque, decreasing from 1.65–1.80 Nm to 1.12–1.25 Nm (Fig. 11), which can be understood given the reduced oil extraction performance and consequently the reduced effort required. What appears more intriguing is the presence of significant cyclical variations in the value of this torque. These variations follow a cycle corresponding to the screw's rotation and indicate changes in the material's resistance during the screw's rotation. These fluctuations are

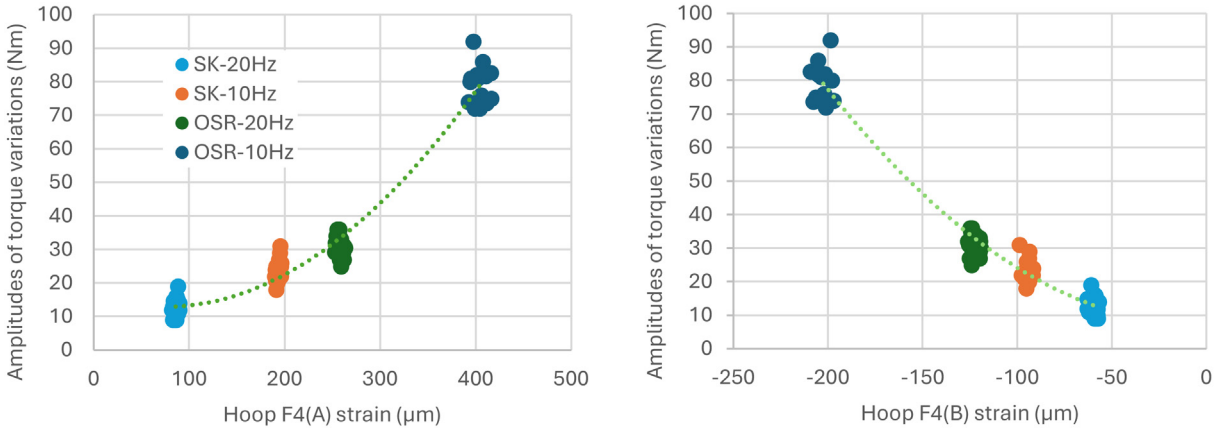

Fig. 11. Relationship between F4 hoop strain (orientation A left and orientation B right) and amplitudes of torque variations.

also observed in the thrust bearing force sensor, although the peaks are not synchronized. These fluctuations share the characteristic of presenting two maxima over one cycle. In the case of torque, these maxima are not symmetrical and are separated by unequal durations (10 seconds between the highest peak and the secondary peak versus 7 seconds from the secondary peak to the main peak).

Initially, we interpreted these torque variations as the effect of changing proximity between the terminal part of the screws and the knives. However, this interpretation fails to account for the asymmetry of the peaks, given that the two half-cages are identical, and the knives are positioned 180° apart from each other. This observation led us to seek an alternative hypothesis by examining correlations between observed parameters and the magnitude of these torque variations. Through this analysis, we discovered a quadratic relationship between hoop strain and the amplitude of torque variations

A Chinese patent describes a method for testing internal stress in screw oil press chambers (CN104723600A, 2015) and mentions that strain can reach several tenth of millimetres. This deformation alters the clearance between the screw and the cage, which consequently affects pressure generation and resistive torque. Given that the pressure at any specific point on the cage varies during the screw's rotation, it is probable that cage deformation is the primary cause of resistive torque variations. Torque is likely to rise when the zone of maximum pressure must pass through the area where the clearance between the screw and cage is at its narrowest. As we observed that the highest tensions on the clamping rings were accompanied by the most significant variations in deformation, it is also possible that the variability of the resistive torque depends on variations in the ovalization of the cage. This ovalization may have an effect similar to that of a clamp whose opening varies by a few tenths of a millimetres.

4.2.3 Effort on the thrust bearing

As mentioned in the results part, the negatives values of the force sensor on the thrust bearing are puzzling and could results from a malfunction of the sensor. While disregarding the absolute values, which do not hold particular significance, we can nonetheless question the cause of thrust variations on the thrust bearing housing. No correlation is found between torque values and thrust pressure when examining variations from one hundredth of a second to the next. However, correlations do exist for rapeseed between thrust and hoop strain F3A with R^2 values of 0.84 and 0.61 at 10 and 20 Hz respectively, which are not observed with sunflower ($R^2 = 0.12$ and 0.09), where the force is generally negative. These correlations disappear for other hoops' strain. Assuming that a physical causality underlies these correlations, it is most probable that the increase in thrust force is the cause of increased cage deformation rather than the inverse. This leaves open the question of what causes the variations in thrust pressure.

4.3 Solid material progression in the press

Two sources of information can enhance our understanding of solid matter movement within the press. The first is the ratio of estimated actual flow rate to potential flow rate for each screw segment, as shown in Table 4 in Rousseau *et al.*, 2025. The second is derived from the modelling of residence time distributions. The first comparison that can be made is that of the transport capacity of screw 'A', which decreases from 63% of the theoretical capacity at 3.5 rpm to 53% at 7 rpm. This decline represents a reduction in the press's processing capacity, occurring despite the fact that the press has a significantly degraded oil yield, which might seem counterintuitive. However, this capacity loss becomes quite logical when examining the same ratios at the level of screw 'K', where at 7 rpm, the screw is traversed by a flow rate exceeding the volume it is supposed to generate. The compression profile is evidently not adapted to this operating speed. The bottleneck is localized at screw 'I', which impedes the advancement of material pushed by upstream screws. Consequently, the solid is forced to move forward more slowly than the screw rotation would allow. The backflow of material results in the rotation of the material with the screw. The question that arises then is whether this rotation concerns only a fraction of the material volume present in the screw or if it's the entire cake that slides on the cage and rotates with the screw.

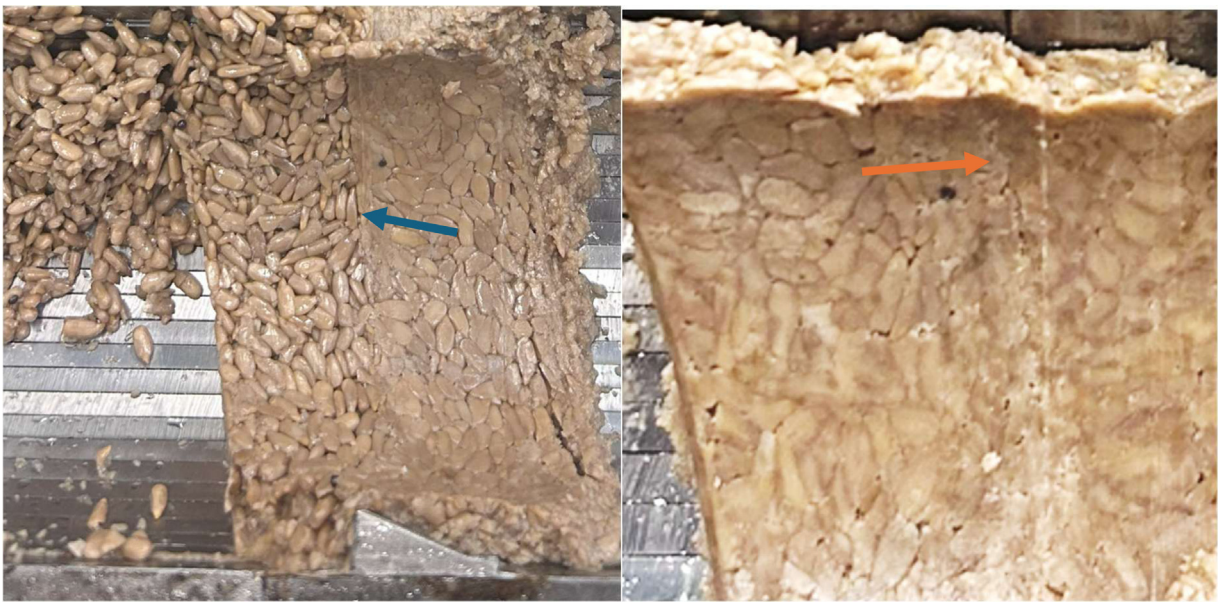

Fig. 12. Manifestations of the material rotation with the screw by two pictures of the press interior. On the left in the area of screw 'C' and cone 'D', on the right in the region of screw 'E' and cone 'F'. The arrows indicate the boundary lines between the area where the cake, retained by the knives, does not rotate with the screw, and the area where it is probably rotating.

The observation of the press interior after opening the press under load, as shown in Figure 12, provides a rather clear indication of what occurs in screw 'C' when the kernels begin to be compressed and form the cake. One can clearly see the line separating the kernels rotating with the screw and the cake that begins to form in cone 'D'. In the cone ring, the cake cannot rotate due to the presence of knives, whereas in the screw channel, the kernels have this capability. Visualizing what happens after the cake is formed is more challenging, as clear boundaries between the rotating and stationary zones are less apparent. It is possible that no distinct separation exists; instead, a gradient of rotation may develop between the non-rotating cone area and the screw channel. The image on the right hints at an irregular fracture line that could be related to the rotation of the cake.

This reflux explains the dispersion of the residence time measured by the tracer. Regarding the remanence of the tracer in the second model it could be explained by the rejection of some marked kernels in the feeding area at the entry of the cage. The screw always empties from the rear, and since the tracer injection was performed when the feed zone was empty, with a layer of unmarked kernels added on top to avoid disturbing the feed, it is probable that the tracer backflow would have stagnated in this area where renewal is slower than at the rear.

Regarding the observation of tracer exiting the press earlier than predicted by plug-flow models, this phenomenon can be interpreted as a consequence of material acceleration induced by passage through the conical rings. The constriction at these points may force the forward extrusion of some material, particularly in the terminal screw segments. These latter sections are likely to be underfed and partially empty, thus facilitating preferential flow paths for a portion of the material. This accelerated transit could explain the premature emergence of tracer, deviating from the idealized plug-flow behaviour.

5 Conclusion

This study offers a detailed, real-time analysis of the mechanical and flow dynamics within screw press during oil extraction from sunflower kernels and rapeseed. By combining high-frequency measurements of pressure, torque, cage deformation, and residence time distribution, the research reveals that internal press dynamics are highly variable and closely tied to the rotation of the screw. Notably, significant fluctuations in pressure and strain were observed, challenging conventional steady-state models and highlighting the need for more sophisticated approaches to describe screw press behaviour.

The comparative analysis between sunflower kernels and rapeseed demonstrates that material properties strongly influence press performance. Sunflower kernels, due to their stronger filtration resistance and higher deformability, result in flatter pressure profiles and reduced energy consumption, but also limit the maximum achievable pressure and oil yield. In contrast, rapeseed generates higher pressures, especially near the press outlet, and requires considerably more torque and energy, reflecting lesser plasticity caused by its hull content. Residence time distribution measurements further indicate complex material flows, including backflow, particularly at higher screw speeds. These findings suggest that traditional plug-flow or perfectly mixed reactor models are insufficient, and that hybrid models accounting for tracer retention and delayed release are more appropriate in the case of SK. The variations of the torque during the revolution related to the cage deformation is an important result that should encourage press manufacturer to reinforce the rigidity of the cage for smoother rotation of the screw and lower energy consumption. Further research should extend these insights to other oilseed types and press configurations to support broader industrial application.

References

Anferov SD, Skul'skiy OI. 2014. Modelling of fluid filtration through plastically deformed porous medium in the process of extrusion. *PNRPU Mech Bull* 2: 29–47.

Bargale P. C, Ford R. J, Sosulski F. W, Wulfsohn D, & Irudayaraj J. (1999). Mechanical oil expression from extruded soybean samples. *J. Am. Oil Chem. Soc* 76: 223–229

Bahadar A, Khan MB, Mehran T. 2013. Design and development of an efficient screw press expeller for oil expression from *Jatropha curcas* Seeds: a computational flow dynamics study of expeller for performance analysis. *Ind. Eng. Chem. Res*. 52: 2123–2129.

Barzegari MR, Almasi A. 2020. Online condition monitoring of industrial twin-screw extruders using motor current signature analysis. *Measurement* 165: 108076.

Bogaert L, Mhemdi H, Vorobiev E. 2020. Residence time distribution and flow pattern modeling of oilseeds in a pilot screw press. *OCL* 27: 65.

Bogaert L, Mathieu H, Mhemdi H, Vorobiev E. 2018. Characterization of oilseeds mechanical expression in an instrumented pilot screw press. *Ind. Crops Products* 121: 106–113.

Booth EJ. 2004. Extraction and refining. *Rapeseed and canola oil* 17–31.

Carré P. 2022. New approach for the elucidation of the phenomena involved in the operation of vegetable oil extraction presses. *OCL* 29: 6.

Future Market Insights. 2023. *Commercial Oil Extraction Market Report*. Retrieved from: https://www.futuremarketinsights.com/reports/commercial-oil-extraction-machine-market. Last consult: May 3, 2025.

Girotto F. 2026. Sunflower press-cake and its protein extract for food applications: effects of sonication on functional properties. *Foods Raw Mater* 14: 117–122.

Karaj S, & Müller J. (2011). Optimizing mechanical oil extraction of Jatropha curcas L. seeds with respect to press capacity, oil recovery and energy efficiency. *Ind. Crop. Prod* 34: 1010–1016

Kovalyshyn S, Tomyuk V. 2018. Research on power consumption of screw press for pressing of oil from rape seed. *BIO Web Conf* 10: 02011.

Kumar Metal. 2025. *Sustainable Extraction Technologies*. Retrieved from « https://kumarmetal.com/setting-up-a-new-plant-how-to-choose-the-most-sustainable-edible-oil-extraction-machine/ », last consult May 3,2025.

Le Clef E, Kemper T. 2015. Sunflower seed preparation and oil extraction. In *Sunflower* (pp. 187–226). AOCS Press.

Li Y, *et al.* 2023. *J Cleaner Prod* 415: 137812.

Pilorgé E. 2020. Sunflower in the global vegetable oil system: situation, specificities and perspectives. *OCL* 27: 34.

Rousseau F, Carré P, Gouyo T, Savoire R. 2025, On the Difficulty of Pressing Hulled Sunflower Seeds: Challenges in Mechanical Oil Extraction, OCL, on press.

Sitek W, Havran V. 2024. Mathematical model of the influence of geometric parameters of the shaft on the productivity of the screw press. *Eng Rev* 125–135.

Tanko B, *et al.* 2023. *Mathematical modeling of mechanical horizontal screw oil extractor. EJounral*.

Uitterhaegen, E., & Evon, P. (2017). Twin-screw extrusion technology for vegetable oil extraction: A review. *J. Food Eng* 212: 190–200

Vadke VS, Sosulski FW. 1988. *J Am Oil Chem Soc* 65: 1619–1627.

Ward JA. 1976. Processing high oil content seeds in continuous screw presses. *J Am Oil Chem Soc* 53: 261–264.

Cite this article as: Carré P, Rousseau F, Gouyo T, Savoire R. 2025. Insights from an Instrumented Screw Press: Investigating pressure, torque, cage strain and flows dynamic. *OCL* 32: 27. https://doi.org/10.1051/ocl/2025023